ACS OMEGA

http://pubs.acs.org/journal/acsodf

Article

Genetic Model of Mud-Clast Conglomerates in Salt Rocks and Their Significance for Salt Mineralization in Mohei Area, Simao Basin, China: A Case Study of Well L-2

Pengcheng Lou, Zhongying Miao,* Mianping Zheng, Nina Ma, Qihui Xu, and Xinmin Li

Cite This: *ACS Omega* 2022, 7, 15547−15560

Read Online

ACCESS | Metrics & More | Article Recommendations

ABSTRACT: The Simao Basin is one of the most important Mesozoic salt basins in China, and the salt rocks generally contain mud-clast conglomerates. The characteristics of mud-clast conglomerates can provide effective information indicating the evolution process of the salt deposits. A combined analysis of trace elements and clay minerals was performed to characterize the genetic model of mud-clast conglomerates in the salt rocks. The results show that the sedimentary materials are felsic rocks from the Upper Crust. Ternary plot diagrams show that the tectonic settings are between the continental margin and the continental island arc. The clay minerals in the samples mainly contain illite and illite−smectite mixed layers. A dry and hot climate prevailed during the deposition of the Mengyejing Formation, and the warm-humid climate that also occurred is interspersed in some periods. Evaporation makes the water bodies shallower, and the concentrated brine starts to precipitate salt under the arid and hot climate conditions. Redox proxies indicate that most of the samples were deposited in relatively oxic conditions. The Sr/Ba ratios (average of 0.5) and paleosalinity (average of ∼35‰) during the depositional period indicate an increase in terrigenous freshwater input and carry of clasts into the evaporation basin. Furthermore, the freshwater supply enhances the hydrodynamics; as a result, the detritus that deposited in the early stage is broken into mud-clast conglomerates and co-deposited with the salt rocks. The results provide a geochemical basis for further study of mud-clast conglomerates in the Simao Basin and supply recommendations for the origin of salt deposits in similar basins around the world.

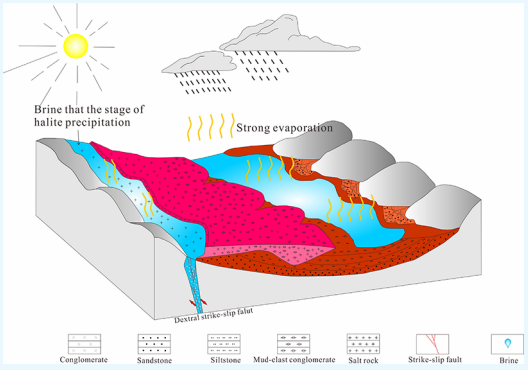

1. INTRODUCTION

The Simao Basin is located in the southeast of the Tethys tectonic domain, which is the important salt and potash salt basin in southwest China.[1,2] The Mengyejing potash salt deposit in the Simao Basin at present is the only known pre-Quaternary solid potash deposit in China. Previous studies have been carried out on sedimentary stratigraphy, petrography, salt sedimentary geochemistry,[3,4] isotopic characteristics,[5−7] salt structure, metallogenic era,[1,8−11] and mineralogical characteristics[12,13] and through relevant research result in understanding of the genesis of the salt deposits in the basin. However, the metallogenic model of the Mengyejing potash deposit has been a subject of debate and controversy: there are viewpoints such as the "marine incursion continental primary sedimentary potash deposit"[3,10,14]—this viewpoint suggested that the potash deposits in the Simao Basin were formed by marine incursion as sources of potash under the continental environment and evaporation of salt under the arid and hot climates; "two-story potash forming model"[1,15,16]—this viewpoint suggested that the genesis of the Mengyejing potash deposit is deep solid salts diapirs triggered by tectonic activities for forming a potash mine at a shallower depth; "deep source and shallow mineralization"[7]—this viewpoint suggested that sources of the deposit are from a deep marine stratum and the metallogenic epoch of the deposit is during the clastic depositional stage of the Mengyejing Formation (MYJ Fm.).

The characteristics of mud-clast conglomerates in the salt can provide effective information indicating the evolution process of brine and reflect environmental changes of the salt deposits.[17,18] It is of great significance for understanding the genetic mechanism of potash deposits. Previous studies on mud-clast conglomerates mainly focused on provenance and paleoclimate.[7,19−22] However, there are a few studies on the genetic model of mud-clast conglomerates, especially mud-clast conglomerates in the salt. The Mohei area is located in the

Received: January 14, 2022
Accepted: April 7, 2022
Published: April 26, 2022

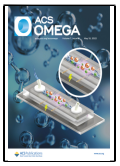

https://doi.org/10.1021/acsomega.2c00292
ACS Omega 2022, 7, 15547−15560

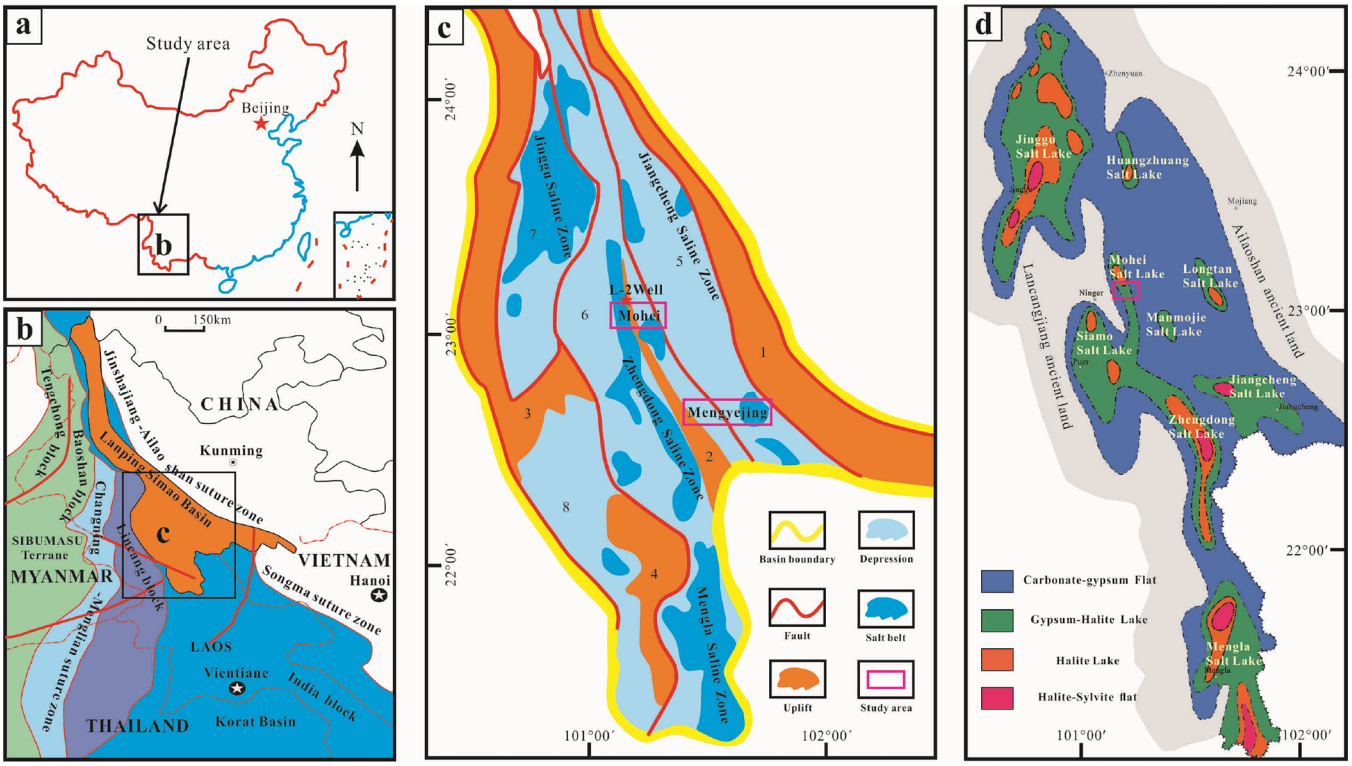

Figure 1. (a) Location map of the Simao Basin. (b) Main structural units around Simao Basin. (c) Distribution of the salt-bearing belt of the Simao Basin. (d) Paleogeographic map of Mengyejing Formation during the depositional period in the Simao Basin. 1, Mojiang Uplift; 2, Yingpanshan Uplift; 3, Jinghong Uplift; 4, Mengyuan Uplift; 5, Jiangcheng Depression; 6, Mohei-Mengla Depression; 7, Jinggu Depression; 8, Dadugang Depression.

middle of the Simao Basin, at the north of the Mohei-Zhengdong salt-bearing belt. It is an important salt resource production base in the basin. However, there are few reports on the genesis of salt deposits in this area.

In this paper, the main research object is the core sample of well L-2 in the Mohei area. This paper focuses on the geochemical characteristics of trace elements, rare earth elements (REE), and the content of clay minerals in the mud-clast conglomerates in the salt rocks. We intend to the analysis of relevant parameters such as element relative content, identification diagram, paleoclimate, and paleoenvironment, identifying the provenance, tectonic background of provenance area, sedimentary conditions, paleoclimate conditions, paleosalinity of mud-clast conglomerates in salt rocks. Furthermore, we constructed the genetic model of mud-clast conglomerates bearing salt rocks, which provides a basis for analyzing the genesis of mud-clast conglomerates in salt rocks and the genesis of salt deposits.

2. GEOLOGICAL SETTING

The Simao Basin is located in the southwest of Yunnan Province, China (Figure 1a). Its tectonic location is in the northwestern Indochina Block (Figure 1b), belonging to the east Tethys tectonic domain. The Simao Basin is a Meso-Cenozoic intracontinental basin developed after the disappearance of Lancangjiang and Jinshajiang and is bounded to the east by the Jinshajiang-Ailaoshan suture zone and to the west by the Lancangjiang suture zone.[23,24] Its north is connected with the Lanping Basin. The southern boundary of the Simao Basin extends to the boundary with the Vientiane Basin and Korat Basin and forms a series of evaporite basins.

The properties of the basin are closely related to the tectonic evolution of the Mesozoic orogenic belt.[25] At the Triassic is a back-arc foreland basin; the Cenozoic is a strike-slip and pull-apart basin affected by the collision between the Indian Plate and the Eurasian plate; after the closure of the Paleo-Tethys continent−continent collision, the Jurassic−Cretaceous period is a continental marginal rift basin. The results of paleomagnetic indicate that the Simao Block and Indochina Block have undergone differential internal rotational deformation since the Cenozoic,[26−28] and the block rotated clockwise from near EW, forming the present NNW.[29]

The Simao Basin can be divided into four uplifts and four depressions, a total of eight secondary tectonic units. The salt deposits discovered so far are developed in the Jinggu Sag, Jiangcheng Sag, and Mohei-Mengla Sag. At present, no salt deposit has been found in the Dadugang Sag (Figure 1c). The paleogeographical pattern of the MYJ Fm. during the depositional period was the Lanping-Simao inland arid plain between the Ailao Mountains and the Lancangjiang Mountains, on which a series of salt lakes developed. The sediments are brown-red mudstone, siltstone, and mud-clast conglomerate, generally containing gypsum-salt rock and local potash. The study area has evolved into the halite lake stage at this period (Figure 1d).

The sedimentary basement of the Simao Basin is the Precambrian-Lower Paleozoic greenschist facies metamorphic complex,[30] and the sedimentary cover fill consists of Mesozoic−Cenozoic strata. Among them, the main lithology of the Triassic is limestone, sandstone, and mudstone; the Middle Jurassic sedimentary fill consists of marine biological limestone; the Upper Jurassic is mainly continental red beds. Due to transgression and regression, the strata in the basin are generally

https://doi.org/10.1021/acsomega.2c00292
ACS Omega 2022, 7, 15547−15560

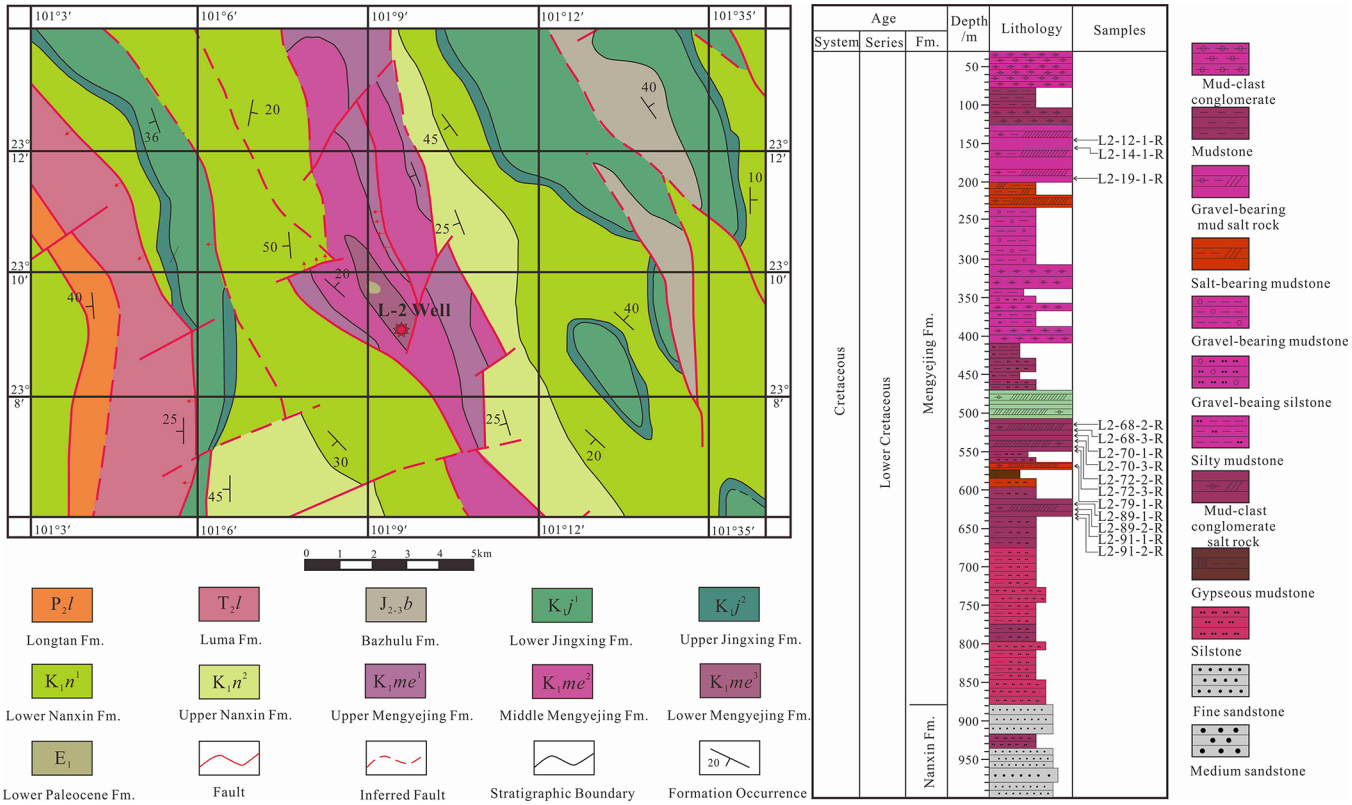

Figure 2. Location of the well L-2, its surrounding geology, and sampling location.

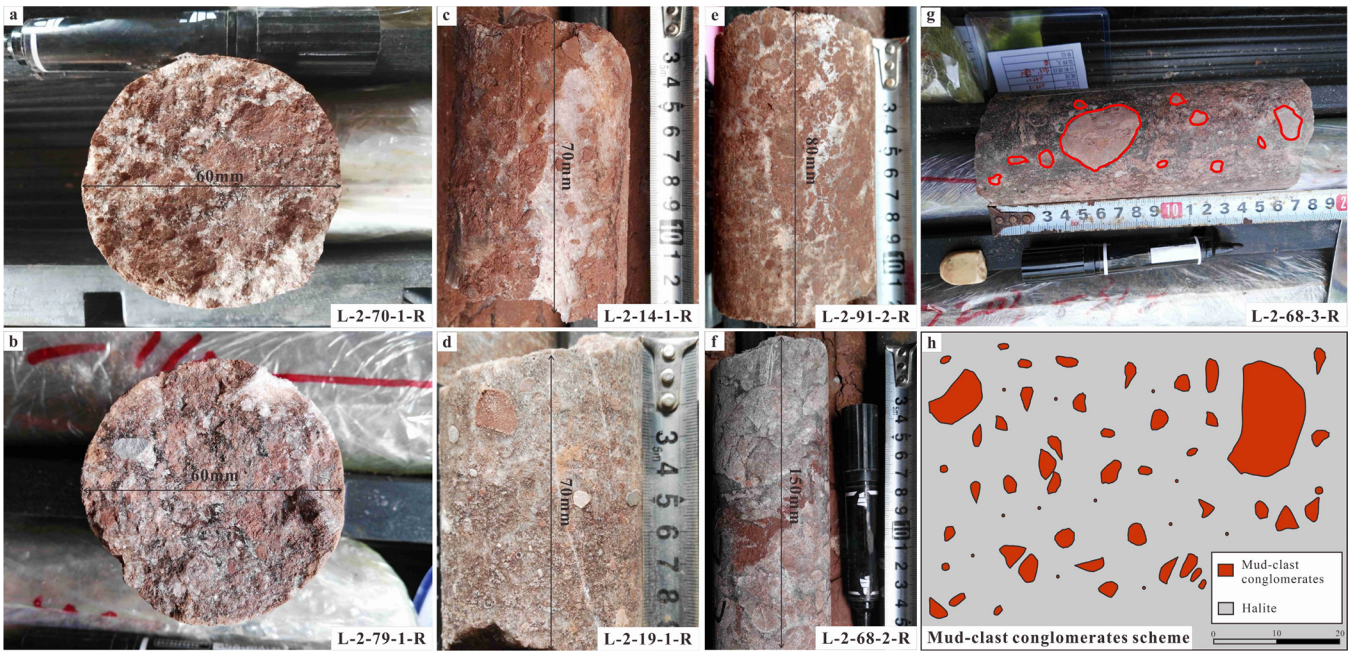

Figure 3. Mud-clast conglomerate-bearing salt rocks of well L-2. (a) L-2-70-1-R, (b) L-2-79-1-R, (c) L-2-14-1-R, (d) L-2-19-1-R, (e) L-2-19-2-R, (f) L-2-69-2-R, (g) L-2-68-3-R. (h) Mud-clast conglomerates scheme image.

characterized by marine facies, marine continental transitional facies, and continental facies combination.[1,25,31] MYJ Fm. is the main occurrence layer of salt rock in the basin. The analysis of the sporopollen record shows that the age of MYJ Fm. is Aptian−Albian and in the uppermost part of the Cretaceous.[32]

The salt-bearing strata of the MYJ Fm. are mainly composed of salt rock deposits (mainly including halite, gypsum, and potash) and fine-grain clastic rocks. The MYJ Fm. can be divided into three members: the lower member consists of an evaporite-bearing (gypsum and anhydrite) succession of red-brown mud-clast conglomerates, mudstones, and sandstones; the middle member is mainly composed of red-brown red siltstone, mudstone, and a small amount of fine sandstone, yellow mudstone, and marlstone intercalation; the upper member is

https://doi.org/10.1021/acsomega.2c00292
ACS Omega 2022, 7, 15547−15560

mainly ore-bearing, including halite, sylvite, and gypsum interbedded with mud-clast conglomerates and siltstones. According to the difference in mineral composition, mud-clast conglomerates can be further divided into silty mud-clast conglomerates, lime mud-clast conglomerates, gypsum mud-clast conglomerates, and salt soluble mud-clast conglomerates.

3. SAMPLES AND METHODS

3.1. Samples. The samples selected in this paper were from well L-2 in the Mohei-Zhengdong salt bearing zone (GPS: 23° 9′ 1.5″ N, 101° 9′ 28.7″ E). MYJ Fm. is exposed around the borehole of L-2, as well as Nanxin Fm. and Jingxing Fm. of the Lower Cretaceous, Bazhulu Fm. and Hepingxiang Fm. of the Jurassic and Luma Fm. of the Upper Triassic are also exposed around the wellhead. The main body develops NW-SE reverse faults with an angle of dip ranging from 40° to 60° (Figure 2).

There are two salt-bearing sections in well L-2, the depth is from 125.87 to 232.25 m and from 469.05 to 721.42 m, and the cumulative thickness of salt-bearing sections by the full-hole is 358.75 m (Figure 2). The diameter of the mud-clast conglomerates in the salt rocks of Well L-2 is distributed between 0.5 and 5 cm, the sorting is not obvious, and most of them are in a breccia shape. Part of the mud-clast conglomerates has a certain roundness and is not directional. Mud-clast conglomerates are randomly distributed in the salt rocks, and the content varies with different parts and the samples primarily with mud-clast conglomerate bearing salt rocks. A total of fourteen samples were selected from a 145 to 632 m depth section (Figure 3). Deionized water was used to fully dissolve the mud-clast conglomerate-bearing salt rocks and extract the water-insoluble matter. The water-insoluble matter was dried in an oven at 60 °C, taken it out, and crushed to 200 meshes for analysis.

3.2. Testing Methods. Before geochemical analyses, all fresh samples were chipped and pulverized (200 mesh). Geochemical samples (250 mg) were analyzed for trace element (Ba, Co, Cr, Cu, Ga, Ni, Rb, Sr, V, Zn, Zr, Th, U, Hf, Sc) concentrations using inductively coupled plasma mass spectrometry (ICP-MS, Thermo Fisher Company, Germany) in the Institute of Geophysical and Geochemical Exploration, Chinese Academy of Geological Sciences. Then, mixed acid solutions of 5 mL of HNO_3 (16.1 mol/L) + 10 mL of HF (22.5 mol/L) + 2 mL of $HClO_4$ (12 mol/L) with geochemical samples were put into a Teflon vessel and heated for decomposition and steam drying at 200 °C. Next, we waited until the sample is completely decomposed and waited again for the samples to cool slightly, then aqua regia of 8 mL of mixed acid of HNO_3 (250 mL) + HCl (750 mL) was added, and the solution was shaken well, then heated on an electric heating plate until 3 to 5 mL of the solution remained, which was heated for 5 to 10 min until the solution was clear and bright. After cooling, the solution was transferred to a polyethylene tube and was diluted with water to 25 mL. Finally, 0.5 mL of the solution was taken, Rh was added as an internal standard and diluted with HNO_3 acid (3 + 97) to 5 mL, and the solution was shaken well and prepared for geochemical analyses. The calculation is corrected, and the error is less than 5%.[33]

A planar grating spectrograph (model: WP-1, Beifen-Ruili Company, China) was used for the determination of boron content. A mixture of NaF, $K_2O_7S_2$, Al_2O_3, GeO_2, and carbon powder was selected as a buffer, germanium as the internal standard element, and alternating current arc as the excitation light source. Two parallel measurements were made by perpendicular electrode emission spectrometry. The average value of the parallel analysis results was used as the content of boron in the samples.

The clay mineral compositions of the samples were analyzed using a Panalytical X'Pert PRO X-ray diffractometer (Panalytical Company, Netherlands). X-ray diffraction traces of oriented sample preparations were scanned between 3° and 30° 2θ at a step size of 0.02° 2θ. Samples were saturated with ethylene glycol and heated at 450 °C for 2.5 h.[34]

4. RESULTS

4.1. Trace Elements. The trace element (B, Ba, Co, Cr, Cu, Ga, Ni, Rb, Sr, V, Zn, Zr, Th, U, Hf, Sc) compositions of samples from the MYJ Fm. are listed in Table 1.

To use trace element concentrations to reconstruct paleoenvironment conditions, one must assess whether they are relatively enriched or depleted. Commonly, the degree of enrichment or depletion of a trace element in a sample is evaluated relative to its concentration in a reference that is commonly the Post Archean Australian Shale (PASS).[35] However, the calcium carbonate and opal in the sedimentary rocks may dilute the abundance of trace elements in a sample. In order to eliminate this effect, it is customary to normalize the trace element concentrations of sedimentary rocks in terms of Al or Th content and express them as enrichment factors.[36−39] In this paper, Th was used to standardize the other trace elements except for boron. The enrichment factors (EF_X) of an element (X) can be expressed as $EF_X = (X/Th)_{Sample}/(X/Th)_{PAAS}$. If EF_X is greater than 1, then the element is enriched relative to average shales; if EF_X is less than 1, it is depleted. This allows an examination of the degree of elemental enrichment in sediment.[35,40]

Table 2 gives values for EF_X from samples. The average enrichment factors of Zn, Ga, Sr, and U are greater than 1, which means that they are relatively enriched. The EF_X of other elements is less than 1, which means that they are relatively depleted (Figure 4).

The boron content of samples from the MYJ Fm. ranges from 70 to 134 ppm, with an average of 101 ppm. The average boron content in shale is 100 ppm, and the average boron content in sandstone is 35 ppm.[41] Compared with the above values, the average boron content of the samples is relatively higher.

4.2. REE. The REE (La, Ce, Pr, Nd, Sm, Eu, Gd, Tb, Dy, Ho, Er, Tm, Yb, Lu) compositions of samples from the MYJ Fm. are listed in Table 3.

The ΣREE of mud-clast conglomerates in MYJ Fm. ranges from 114.72 to 150.06 ppm, where the average value is 135.45 ppm, lower than the average value of North American Shale Composite (NASC) (163 ppm). It is close to the average content in the Upper Crust (146 ppm). The value of light rare earth elements (LREE) ranges from 102.29 to 134.21 ppm, where the average value is 101.24 ppm; the value of heavy rare earth elements (HREE) ranges from 11.13 to 16.33, where the average value is 14.21 ppm. The values of ΣLREE/ΣHREE range from 7.75 to 9.79, where the average value is 8.58. After the NASC-normalized REE, the values of δEu ranges from 0.87 to 0.94, where the average value is 0.89; the value of δCe ranges from 0.93 to 0.96, where the average value is 0.94; the value of La_N/Yb_N ranges from 1.06 to 1.45, where the average value is 1.18. After the chondrite-normalized REE, the value of δEu ranges from 0.56 to 0.61, where the average value is 0.58; the values of δCe range from 0.96 to 0.99, where the average value is

https://doi.org/10.1021/acsomega.2c00292
ACS Omega 2022, 7, 15547−15560

Table 1. Trace Element Contents (Ppm) of the MYJ Fm. of Well L-2, Simao Basin[a]

samples	lithology	depth/m	B	V	Cr	Co	Ni	Cu	Zn	Ga	Rb	Sr	Ba	Zr	Th	U	Hf	Sc
L2-12-1-R	M.C.	145.03	130.0	78.0	57.3	11.3	31.4	21.2	72.2	14.4	87.0	298.0	277.0	59.5	8.8	3.3	1.7	10.3
L2-14-1-R	M.C.	155.12	69.6	79.5	61.9	13.6	30.3	14.5	59.2	15.1	106.0	60.5	267.0	66.7	10.4	3.1	2.0	10.7
L2-19-1-R	M.C.	198.96	110.0	77.9	57.8	10.9	30.2	24.6	62.8	14.4	89.1	157.0	268.0	62.7	9.1	8.0	1.8	10.6
L2-68-2-R	M.C.	514.08	110.0	82.8	60.4	11.4	29.3	27.8	65.1	14.7	92.5	111.0	283.0	97.8	10.4	4.9	2.9	11.2
L2-68-3-R	M.C.	517.49	134.0	78.4	57.6	10.5	28.7	29.0	108.0	14.5	84.1	158.0	268.0	103.0	9.8	4.1	2.9	11.0
L2-70-1-R	M.C.	523.20	79.0	82.7	62.2	12.2	29.5	24.5	90.1	15.2	110.0	95.3	234.0	102.0	10.7	4.1	3.3	11.9
L2-70-3-R	M.C.	532.30	104.0	78.9	58.4	11.2	29.2	38.8	121.0	14.8	91.9	147.0	273.0	116.0	10.5	4.4	3.2	11.0
L2-72-2-R	M.C.	543.91	104.0	79.2	57.6	11.0	28.4	50.3	105.0	14.3	93.0	173.0	276.0	109.0	10.2	3.9	3.0	11.1
L2-72-3-R	M.C.	545.35	97.8	76.1	57.0	10.9	29.7	36.4	168.0	14.1	88.8	163.0	296.0	108.0	10.1	4.4	3.0	11.0
L2-79-1-R	M.C.	571.47	98.3	81.6	61.9	11.8	30.8	33.0	94.5	15.4	108.0	153.0	446.0	110.0	10.6	4.3	3.2	11.5
L2-89-1-R	M.C.	613.36	100.3	82.8	60.3	11.3	30.1	36.4	92.0	14.8	92.2	197.0	308.0	83.5	9.9	5.4	2.4	10.8
L2-89-2-R	M.C.	615.70	104.0	79.6	59.9	11.2	28.4	23.6	86.6	14.8	86.4	128.0	257.0	89.0	9.8	4.2	2.6	11.1
L2-91-1-R	M.C.	628.54	89.5	72.7	52	10.8	27.3	20.8	87.9	13.4	89.1	139.0	273.0	94.5	8.8	3.7	2.3	10.2
L2-91-2-R	M.C.	631.78	89.4	75.6	53.4	11.3	32.1	20.4	72.8	13.8	111.0	212.0	472.0	99.6	11.0	3.8	3.1	10.8
mean			101.4	79.0	58.4	11.4	28.0	29.7	91.8	14.6	94.9	156.6	299.9	93.0	10.0	4.4	2.7	10.9
PASS		/	150	110	23	55	50	85	20	160	200	650	210	15	3	5	16	

[a]PASS date according to Taylor and Mclennan.[42] M.C., mud-clast conglomerates.

0.98; the value of La_N/Yb_N ranges from 8.09 to 11.04, where the average value is 9.00.

4.3. Clay Minerals. The results derived from semi-quantitative clay mineralogical analysis of the studied samples are listed in Table 4. The bulk composition for all the studied samples is mainly formed of illite, illite−smectite mixed layer (I/S), and chlorite.

5. DISCUSSION

5.1. Provenance Properties of Mud-Clast Conglomerates. The REE distribution patterns of the sedimentary rock can provide meaningful information regarding provenance and the sedimentary environment.[45,46] There are two ways to study the REE distribution patterns of sedimentary rocks: one is to normalize by the chondrite, which has been considered as the original material of the earth, so chondrite standardization can reflect the differentiation degree of samples relative to the original material of the earth and explain the characteristics of the sediment source region; the second is to normalize by the NASC to understand the influence and differentiation degree of mixing and homogenization in the process of sedimentation.

According to Table 3 and the corresponding calculation results, Figure 5a is the normalized REE distribution pattern of chondrite. The REE from the Upper Crust of the continent is characterized by LREE enrichment, stable HREE content, and negative Eu anomaly.[47,48] If the parent rocks of clastic sediments originate from the Upper Crust, the REE distribution pattern should be consistent with that of the Upper Crust.[49] From the shape of the curve, all the samples have the characteristics of a Eu negative anomaly and Ce negative anomaly with enrichment of LREE and deficient of HREE, and the distribution pattern is the same as that of the Upper Crust. Generally speaking, the MYJ Fm. has the characteristics of homology, the provenance is stable in the process of deposition, and its original material should come from the Upper Crust. Figure 5b shows the normalized distribution pattern of shale in NASC. The pattern curves of most samples are similar, that is, a gentle curve slightly to the right, showing LREE enrichment and HREE deficiency. It is characterized by a slight negative Eu anomaly and a slight negative Ce anomaly. It reflects that the sedimentary environment is an oxidation environment. The overall curve is relatively flat, indicating that there is no obvious difference between the mud-clast conglomerates in the salt rock of MYJ Fm. and NASC.

Shields and Stille[50] believe that diagenesis can change the Ce anomaly value, the result will be negative the value of δCe, and δEu has a good negative correlation. There is an apparent positive correlation between the value of δCe and REE. Mud-clast conglomerates of MYJ Fm. in well L-2, and the correlation coefficient of the value of δCe and δEu is 0.07; the correlation coefficient of δCe and REE is 0.17. It shows that diagenesis has a limited influence on REE of mud-clast conglomerates in MYJ Fm., so it should be reliable to use REE characteristics to reflect source attributes.

Trace elements in detritus can provide information about the provenance properties of sedimentary rocks. The comparison of characteristic trace element ratios of MYJ Fm. clastic rocks and crustal elements (Table 5) shows that the element characteristic values of mud-clast conglomerates are close to those of the upper continental crust but far from those of the lower continental crust and oceanic crust. To further reveal the parent rock attributes, the samples were mapped by using Hf-La/Th (Figure 6a),[52] La/Sc-Co/Th (Figure 6b),[53] La/Yb-REE (Figure 6c),[54] and Th/Sc-Zr/Sc (Figure 6d)[55] parent rock attribute discrim-

https://doi.org/10.1021/acsomega.2c00292
ACS Omega 2022, 7, 15547−15560

Table 2. Enrichment Factors of Trace Element of MYJ Fm. of Well L-2, Simao Basin

samples	lithology	depth/m	V	Cr	Co	Ni	Cu	Zn	Ga	Rb	Sr	Ba	Zr	U	Th	Hf	Sc
L2-12-1-R	M.C.	145.03	0.86	0.86	0.81	0.95	0.70	1.41	1.19	0.90	2.47	0.71	0.47	1.82	0.60	0.56	1.07
L2-14-1-R	M.C.	155.12	0.74	0.79	0.83	0.77	0.41	0.98	1.06	0.93	0.42	0.58	0.45	1.45	0.71	0.56	0.94
L2-19-1-R	M.C.	198.96	0.83	0.84	0.76	0.88	0.79	1.18	1.15	0.89	1.26	0.66	0.48	4.27	0.62	0.58	1.06
L2-68-2-R	M.C.	514.08	0.77	0.77	0.70	0.75	0.78	1.08	1.03	0.81	0.78	0.61	0.65	2.29	0.71	0.81	0.98
L2-68-3-R	M.C.	517.49	0.78	0.78	0.68	0.78	0.86	1.89	1.08	0.78	1.17	0.61	0.73	2.03	0.67	0.86	1.02
L2-70-1-R	M.C.	523.20	0.75	0.77	0.72	0.73	0.67	1.45	1.04	0.94	0.65	0.49	0.66	1.86	0.73	0.90	1.01
L2-70-3-R	M.C.	532.30	0.73	0.74	0.68	0.74	1.08	1.98	1.03	0.80	1.02	0.58	0.77	2.04	0.72	0.89	0.96
L2-72-2-R	M.C.	543.91	0.76	0.75	0.68	0.74	1.44	1.77	1.02	0.83	1.24	0.61	0.74	1.86	0.70	0.86	0.99
L2-72-3-R	M.C.	545.35	0.73	0.75	0.69	0.78	1.05	2.86	1.02	0.80	1.18	0.66	0.74	2.12	0.69	0.87	0.99
L2-79-1-R	M.C.	571.47	0.75	0.78	0.71	0.77	0.91	1.53	1.06	0.93	1.05	0.95	0.72	1.97	0.73	0.88	0.99
L2-89-1-R	M.C.	613.36	0.81	0.81	0.72	0.80	1.07	1.59	1.09	0.85	1.45	0.70	0.58	2.65	0.68	0.71	0.99
L2-89-2-R	M.C.	615.70	0.79	0.81	0.72	0.77	0.70	1.51	1.10	0.80	0.95	0.59	0.63	2.08	0.67	0.77	1.03
L2-91-1-R	M.C.	628.54	0.80	0.78	0.78	0.82	0.69	1.71	1.11	0.92	1.15	0.69	0.74	2.04	0.61	0.76	1.05
L2-91-2-R	M.C.	631.78	0.67	0.64	0.65	0.77	0.54	1.14	0.92	0.92	1.41	0.96	0.63	1.68	0.75	0.82	0.90
mean			0.77	0.78	0.72	0.79	0.84	1.58	1.06	0.86	1.16	0.67	0.64	2.16	0.69	0.77	1.00

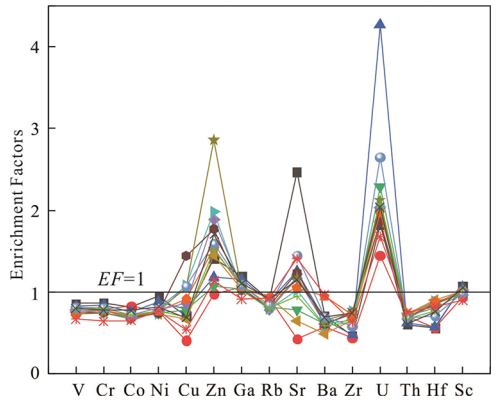

Figure 4. Enrichment factors of trace elements in mud-clast conglomerates in well L-2.

ination diagrams. Most of the samples in Figure 6a fall into the source area of the felsic and basic mixture, and most of the samples in Figure 6d fall into the source area of felsic volcanic rocks. For Co/Th (Figure 6b), the date displays low and relatively constant Co/Th ratios with an average of 1.14, also

Table 4. Relative Contents of Clay Minerals in MYJ Fm. of Well L-2, Simao Basin[a]

			results (wt %)			
samples	lithology	depth/m	I/S	illite	chlorite	RML (S%)
L2-12-1-R	M.C.	145.03	28	46	26	9
L2-14-1-R	M.C.	155.12	39	50	11	9
L2-19-1-R	M.C.	198.96	34	44	22	6
L2-68-2-R	M.C.	514.08	15	57	28	7
L2-68-3-R	M.C.	517.49	40	39	21	9
L2-70-1-R	M.C.	523.20	46	43	11	10
L2-70-3-R	M.C.	532.20	40	42	18	9
L2-72-2-R	M.C.	543.91	36	45	19	9
L2-72-3-R	M.C.	545.35	49	39	12	9
L2-79-1-R	M.C.	571.47	36	46	18	10
L2-89-1-R	M.C.	613.36	38	43	19	9
L2-89-2-R	M.C.	615.70	32	44	24	9
L2-91-1-R	M.C.	628.54	49	38	13	10
L2-91-2-R	M.C.	631.78	39	49	12	10
	mean		37	45	18	9

[a]I/S, illite−smectite mixed layer. RML, ratio of mixed layer.

Table 3. Rare Earth Element Contents (ppm) of Mud-Clast Conglomerates of MYJ Fm. of Well L-2, Simao Basin[a]

samples	lithology	depth/m	La	Ce	Pr	Nd	Sm	Eu	Gd	Tb	Dy	Ho	Er	Tm	Yb	Lu
L2-12-1-R	M.C.	145.03	25.40	49.20	5.90	23.30	4.43	0.75	3.40	0.56	2.92	0.55	1.54	0.27	1.65	0.24
L2-14-1-R	M.C.	155.12	31.10	60.50	7.41	28.80	5.47	0.93	4.60	0.84	4.47	0.82	2.19	0.37	2.24	0.32
L2-19-1-R	M.C.	198.96	24.10	48.40	5.93	23.70	4.51	0.77	3.48	0.59	3.05	0.58	1.60	0.29	1.80	0.24
L2-68-2-R	M.C.	514.08	30.40	57.10	6.83	26.40	4.93	0.84	4.25	0.74	4.03	0.79	2.22	0.40	2.58	0.36
L2-68-3-R	M.C.	517.49	29.00	54.10	6.40	24.70	4.68	0.80	3.89	0.69	3.81	0.72	2.06	0.37	2.42	0.33
L2-70-1-R	M.C.	523.20	31.50	59.90	7.15	27.90	5.15	0.89	4.37	0.77	4.36	0.85	2.42	0.42	2.77	0.38
L2-70-3-R	M.C.	532.20	30.70	56.70	6.80	26.10	4.90	0.83	4.08	0.71	3.93	0.78	2.16	0.40	2.53	0.36
L2-72-2-R	M.C.	543.91	29.80	55.60	6.55	24.80	4.72	0.80	3.92	0.69	3.81	0.75	2.11	0.39	2.40	0.34
L2-72-3-R	M.C.	545.35	28.40	53.90	6.46	25.00	4.63	0.83	3.90	0.68	3.80	0.74	2.13	0.39	2.41	0.33
L2-79-1-R	M.C.	571.47	31.90	60.10	7.06	27.40	5.04	0.91	4.18	0.76	3.98	0.79	2.23	0.42	2.58	0.37
L2-89-1-R	M.C.	613.36	28.50	55.00	6.70	25.40	4.79	0.78	3.75	0.63	3.31	0.65	1.83	0.33	2.10	0.29
L2-89-2-R	M.C.	615.70	29.20	54.70	6.58	25.20	4.67	0.79	3.87	0.68	3.66	0.72	2.07	0.38	2.35	0.32
L2-91-1-R	M.C.	628.54	23.20	45.80	5.69	22.50	4.33	0.77	3.58	0.63	3.34	0.63	1.72	0.31	1.95	0.27
L2-91-2-R	M.C.	631.78	29.90	55.20	6.58	26.00	4.95	0.93	4.31	0.76	4.27	0.82	2.35	0.43	2.65	0.37
mean			28.79	54.73	6.57	25.51	4.80	0.83	3.97	0.69	3.77	0.73	2.05	0.37	2.32	0.32
chondrite			0.24	0.61	0.10	0.47	0.15	0.06	0.21	0.04	0.25	0.06	0.17	0.03	0.17	0.03
NASC			31.50	66.50	7.90	27.00	5.90	1.18	5.20	0.79	5.80	1.04	3.40	0.50	2.97	0.44

[a]Chondrite date according to Boynton.[43] NASC date according to Haskin and Haskin.[44]

https://doi.org/10.1021/acsomega.2c00292
ACS Omega 2022, 7, 15547−15560

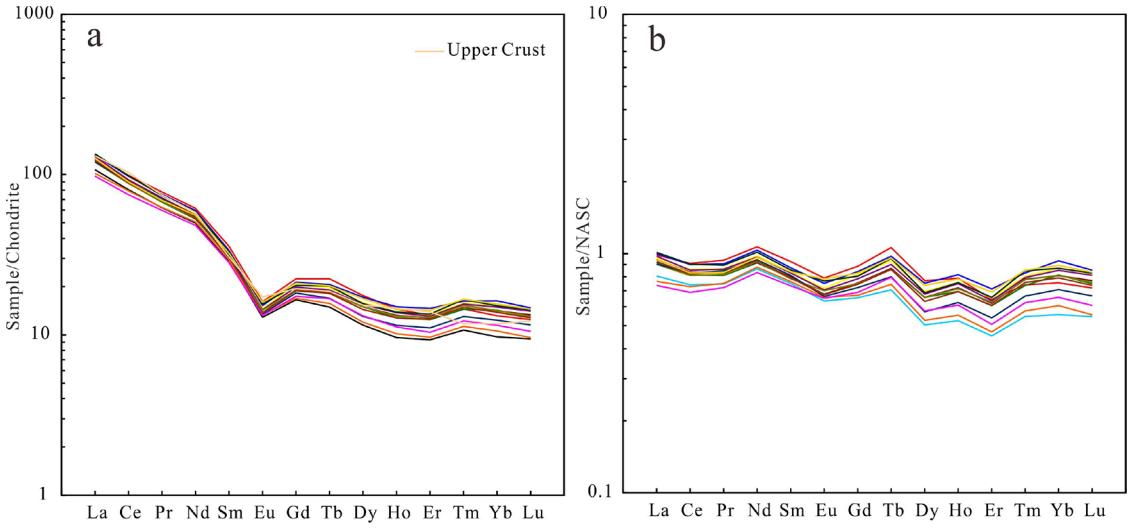

Figure 5. Chondrite-normalized (a) and NASC-normalized (b) REE of MYJ Fm. samples in well L-2.

Table 5. Elemental Ratios of the Samples from Well L-2[a]

source	La/Sc	Sc/Th	Cr/Th	Co/Th	δEu
UCC	2.70	1.00	3.30	0.90	0.61
LCC	0.30	34.0	222	33.0	1.07
OC	0.10	1.73	1227	214	1.02
L-2	2.63	1.10	5.71	1.14	0.58

[a]UCC, upper continental crust. LCC, lower continental crust. OC, oceanic crust.[51]

suggesting dominantly felsic source rocks. Also, most of the samples in Figure 6c fall into the granite area. In conclusion, the parent rock composition of the mud-clast conglomerates in the MYJ Fm. in the Simao Basin is derived from felsic igneous rocks and the upper continental crust.

5.2. Geologic Structure Background of Mud-Clast Conglomerates. Bhatia and Crook[56] studied the REE characteristics of sandstone formed under different structural backgrounds. The characteristics of REE in the sandstone under different source areas are established (Table 6). The results show that the ΣREE in the mud-clast conglomerates of MYJ Fm. in well L-2 is close to the average value of La/Yb in the continental island arc, which is the same as that of the active continental margin. The average value of $(La/Yb)_N$ is 9.0, which

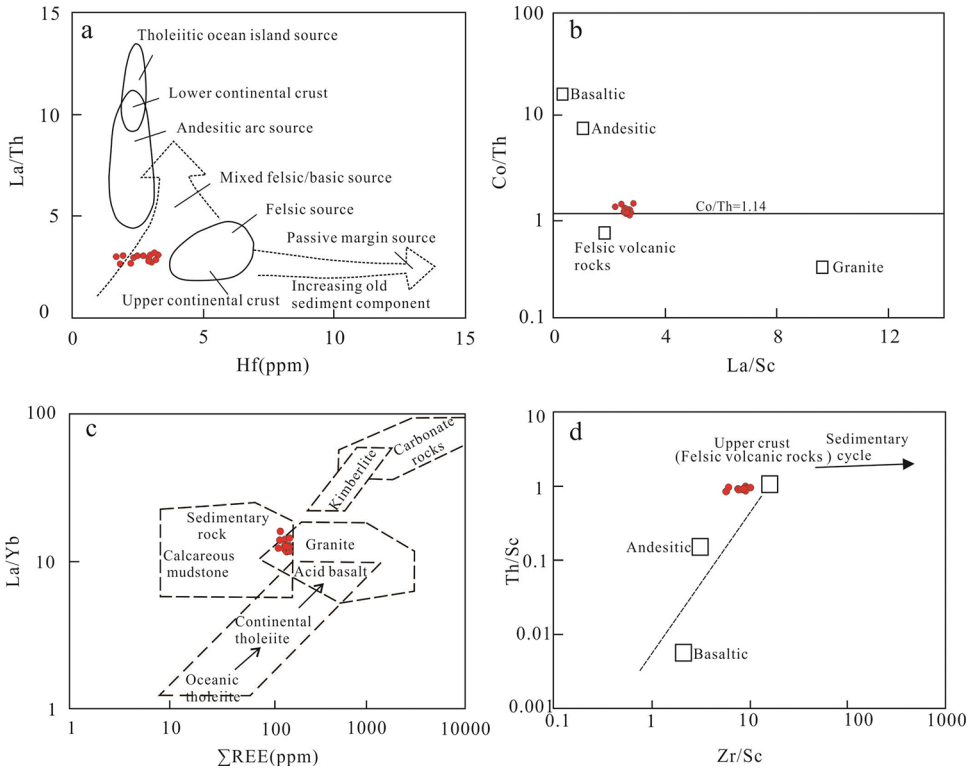

Figure 6. Relationships of Hf-La/Th (a), La/Sc-Co/Th (b), La/Yb-REE (c), and Th/Sc-Zr/Sc(d) of the mud-clast conglomerates from well L-2, Simao Basin.

https://doi.org/10.1021/acsomega.2c00292
ACS Omega 2022, 7, 15547−15560

Table 6. Comparison of REE Characteristic Parameters from Well L-2 with Clastic Rocks in Different Tectonic Settings[a]

source	La (ppm)	Ce(ppm)	ΣREE	La/Yb	$(La/Yb)_N$	L/H	δEu
OIA	8.0	19.0	58.0	4.2	2.8	3.8	1.0
CIA	27.0	59.0	146.0	11.0	7.5	7.7	0.8
ACM	37.0	78.0	186.0	12.5	8.5	9.1	0.6
PM	39.0	85.0	210.0	15.9	10.8	8.5	0.6
L-2	28.8	54.7	135.5	12.5	9.0	8.6	0.6

[a]Note: Date according to Bhatia and Crook,[56] δEu = Eu*/Eu = $Eu_N/1/2 \times (Sm_N + Gd_N)$. OIA, oceanic island arc; CIA, continental island arc; ACM, active continental margin; PM, passive margin; L/H-LREE/HREE.

is close to the average value of active continental margin; the average content of Ce is 54.7, which is not different from that of the island arc; it has the negative abnormal characteristics of Eu.

To further reveal the structural properties of parent rocks, the La-Th-Sc, Th-Sc-Zr, and Th-Co-Zr discrimination diagrams are used to analyze the mud-clast conglomerates in MYJ Fm. (Figure 7).[56,57] The results show that on the La-Th-Sc and Th-Sc-Zr diagrams, most of the samples have the characteristics of a continental island arc, while on the Th-Co-Zr diagram, the samples fall on the active continental margin. The discrimination diagrams of La-Th-Sc, Th-Sc-Zr, and Th-Co-Zr show that the tectonic setting of the mud-clast conglomerates of MYJ Fm. in the study area should be between the continental island arc and the continental margin. In conclusion, the provenance of sediments in MYJ Fm. may be provided by active continental margin and continental island arc.

5.3. Paleoclimate of the Mud-Clast Conglomerate Depositional Period. The relative contents of some trace elements are often used to analyze paleoclimate. In general, the values of Sr/Cu > 5.0 and Ga/Rb are relatively lower in an arid and hot climate,[58,59] and the Sr/Cu ratio values range from 1.3 to 5.0 in the warm and humid climate.[45,60,61] The Ga/Rb values in MYJ Fm. of well L-2 ranges from 0.12 to 0.17, with an average value of 0.15. The Sr/Cu ratio ranges from 3.44 to 14.06, with an average value of 5.87, showing a dry paleoclimate condition and a warm and humid climate condition in individual periods.

The content of clay minerals can be used as a climate index,[62] in which illite and illite−smectite mixed layers represent the arid and semi-arid climate conditions and kaolinite represents the humid climate with a high weathering degree.[63,64] The clay minerals in the mud-clast conglomerates of MYJ Fm. are mainly I + C + I/S type. The illite content ranges from 38 to 57 wt %, and the average value is 45 wt %. The content of illite/smectite mixed layers is between 15 and 49 wt %, with an average value of 37 wt %. The abundance of illite and illite−smectite mixed layers in all samples is suggestive of the prevailing of stable hot and dry paleoclimate conditions during the formation of the MYJ Fm. sediments.

Our understanding of the paleoclimatic conditions of the MYJ Fm. during the sedimentary period is indirectly obtained through the qualitative and quantitative analysis of the clay minerals and relative content of elements in the MYJ Fm. of well L-2. During the Cretaceous, the Simao Basin was located between 21.2° and 28.8° N.[65] The paleoclimate in this latitude zone was mainly dry and hot,[66] with evaporite and calcareous conglomerates (Figure 8). According to the results of geochemical analysis, it is considered that the paleoclimate condition of MYJ Fm. was hot and dry. This understanding is also consistent with the conclusions of sporopollen records,[32] paleogeography, and fluid inclusion thermometry.[67]

5.4. Redox Conditions of Mud-Clast Conglomerate Depositional Period. The solubility of redox-sensitive elements in the sedimentary water is controlled by the redox state of the sedimentary environment, showing the phenomenon of continuous migration and autogenous enrichment to the reducing water and sediment. V, Cr, Co, Ni, and other redox-sensitive elements are easily soluble in the oxidation condition and insoluble in the reduction condition in the sedimentary environment and are autogenous and enriched in the oxygen-poor environment. Compared with Cr, V is easier to be adsorbed and precipitated by colloidal particles and clay in the reduction environment. Ni is mainly enriched in the form of sulfide precipitation in a reduction state, so its ratio can be used as an indicator of the oxidation−reduction state. It is generally believed that the V/Cr value greater than 4.25 and Ni/Co value greater than 7 indicate an anoxic environment. The values of V/Cr ranges from 2 to 4.25 and Ni/Co ranges from 5.0 to 7.0, indicating a weak oxidation environment with weak stratification. The V/Cr value less than 2 and Ni/Co value less than 5 indicates that the water body is an oxidation environment.[69] The V/Cr ratio of MYJ Fm. in well L-2 ranges from 1.28 to 1.44, with an average of 1.36, which indicates that the samples were in an oxidation environment during the depositional period. The Ni/Co ratio ranges from 2.23 to 2.84, with an average of 2.61, indicating the oxidation environment.

According to the difference of U and Th behavior, the U/Th value can also be used as a parameter to identify the redox environment. Generally, a U/Th value greater than 1.25 represents an anoxic environment, a U/Th value between 0.75 and 1.25 represents a weak oxidation environment and subreducing environment, and a U/Th value less than 0.75 represents an oxidation environment;[70−74] the U/Th values of

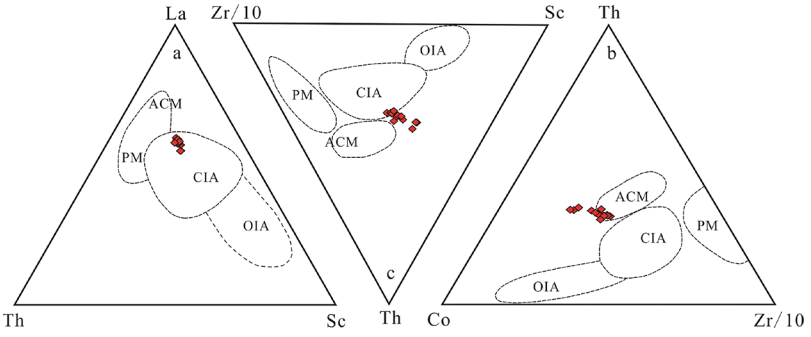

Figure 7. Tectonic setting discrimination diagrams of the mud-clast conglomerates based on La-Th-Sc (a), Th-Co-Zr (b), and Th-Sc-Zr (c).

https://doi.org/10.1021/acsomega.2c00292
ACS Omega 2022, 7, 15547−15560

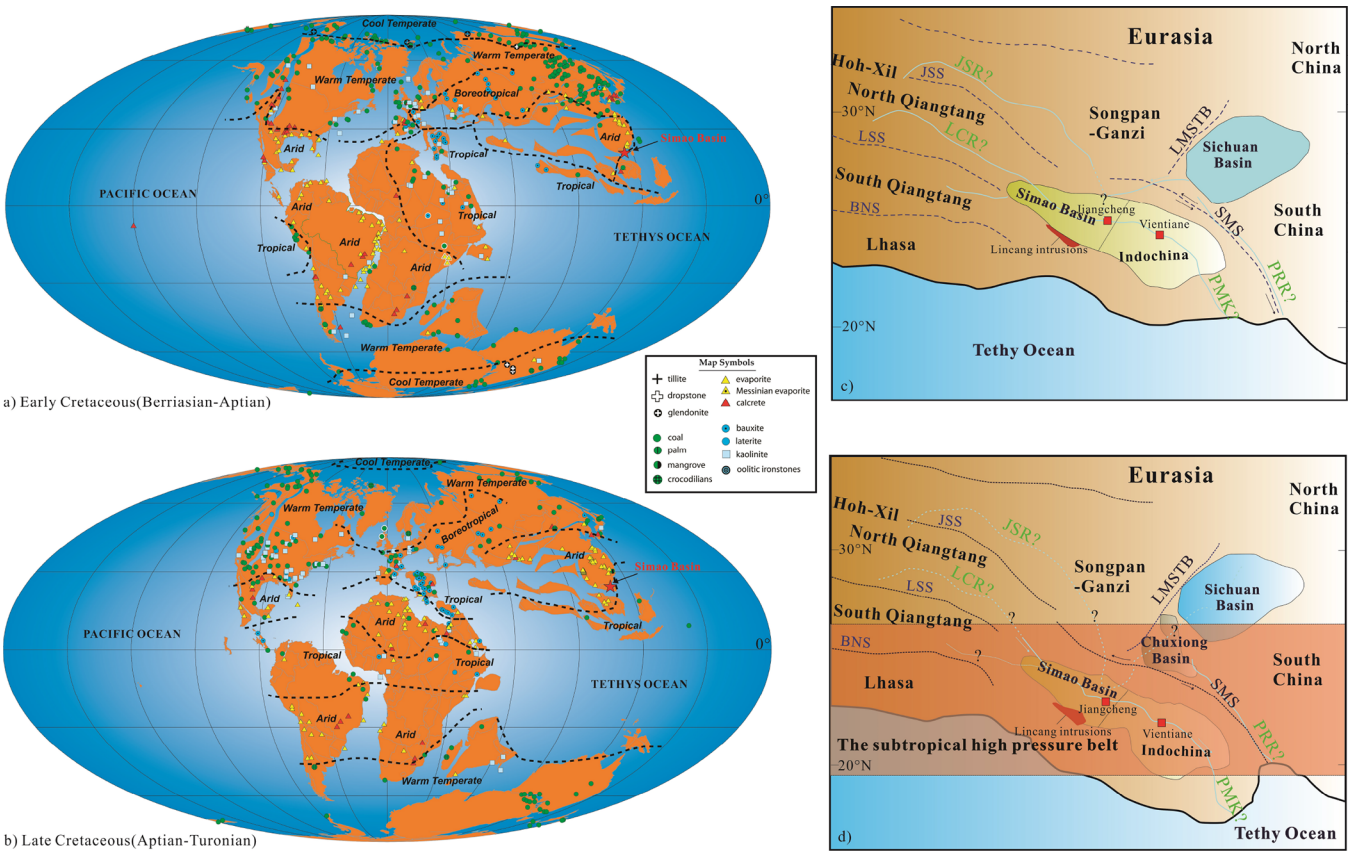

Figure 8. Outline of global Cretaceous paleoclimate zoning (base map adapted with permission from ref 68. (a) Early Cretaceous (Berriasian−Aptian). (b) Late Cretaceous (Aptian−Turonian). (c,d) Schematic regional paleogeography map during the Early and Late Cretaceous (adapted with permission from ref 11. JSR, Jinsha River; LCR, Lancang River; LMSTB, Longmenshan thrust belt; PRR, Paleo-Red River; PMK, Paleo-Mekong River; SMS, Song Ma suture; BNS, Bangong-Nujiang suture; JSS, Jinshajiang suture; LSS, Longmu Co-Shuanghu suture. Science China Press and Springer-Verlag GmbH Germany, part of Springer Nature 2021).

MYJ Fm. samples in well L-2 ranges from 0.30 to 3.09, with an average of 0.62, reflecting the oxidation environment.

V and Ni are also iron group elements. Their ionic valence state changes with the degree of oxidation and is mainly adsorbed and precipitated by colloidal particles or clay, but V is easy to be absorbed and enriched in the oxidation environment while Ni is more easily enriched in the reduction environment. Therefore, the V/(V + Ni) value can reflect the redox environment of the sedimentary water.[73,75] The high ratio (0.84−0.89) reflects the anaerobic environment of water stratification and H_2S in the bottom water. The medium ratio (0.54−0.82) is an anoxic environment with weak stratification. The low ratio (0.46−0.60) is the oxidation environment. The V/(V + Ni) value of clastic rocks in MYJ Fm. of well L-2 is distributed between 0.70 and 0.76, with an average value of 0.73, which reflects the weak oxidation environment.

The above discriminant indexes are selected for parameter intersection (Figure 9). Most of the samples in Figure 9a,b are located in an oxidation environment, and only L2-19-1-R is located in a weak oxidation environment, which can intuitively show that the mud-clast conglomerate in the salt rock depositional period of MYJ Fm. is mainly an oxidation environment. The V/(V + Ni) ratio was used as the discriminant index, and cross plots were made with other redox parameters (Figure 9c,d). It can be seen that the results tend to be in the weak oxidation environment. Therefore, based on all the above analysis results, it can be seen that during the period of mud-clast conglomerates in the salt rocks of MYJ Fm., the water bodies in the Mohei area of the Zhengdong salt-bearing belt in the Simao Basin are previously in an oxidation sedimentary environment.

5.5. Paleosalinity of the Mud-Clast Conglomerate Depositional Period. The deposition of salt mainly depends on the salinity of water bodies, so the salinity of ancient water bodies is an important index to judge the deposition of salt. According to the migration ability of strontium and the geochemical properties of barium, the ratio value of Sr/Ba can be used as a sensitive indicator of paleosalinity. In addition, the regularity of the Sr/Ba value is strong, which reflects that the water quality is the same, that is, the Sr/Ba value is positively correlated with paleosalinity. Generally, the value of Sr/Ba in freshwater sediments is less than 1 while that in saltlake sediments is more than 1. The Sr/Ba values of MYJ Fm. in well L-2 range from 0.10 to 1.08, with an average of 0.50. Therefore, it is inferred that the mud-clast conglomerates of MYJ Fm. were deposited in a freshwater environment.

Boron in sediments mainly exists in clay minerals, which may replace silicon or aluminum atoms in the lattice of clay minerals, and its content is mainly controlled by the boron content in sedimentary water bodies, the content of parent boron. The concentration of boron in sediment water is linearly related to salinity, so the salinity of sediment water can be recovered by boron content in the sediment.

The relationship between boron content in sediments and salinity of sedimentary water bodies can be expressed as follows (Freundlich isothermal adsorption equation):

https://doi.org/10.1021/acsomega.2c00292
ACS Omega 2022, 7, 15547−15560

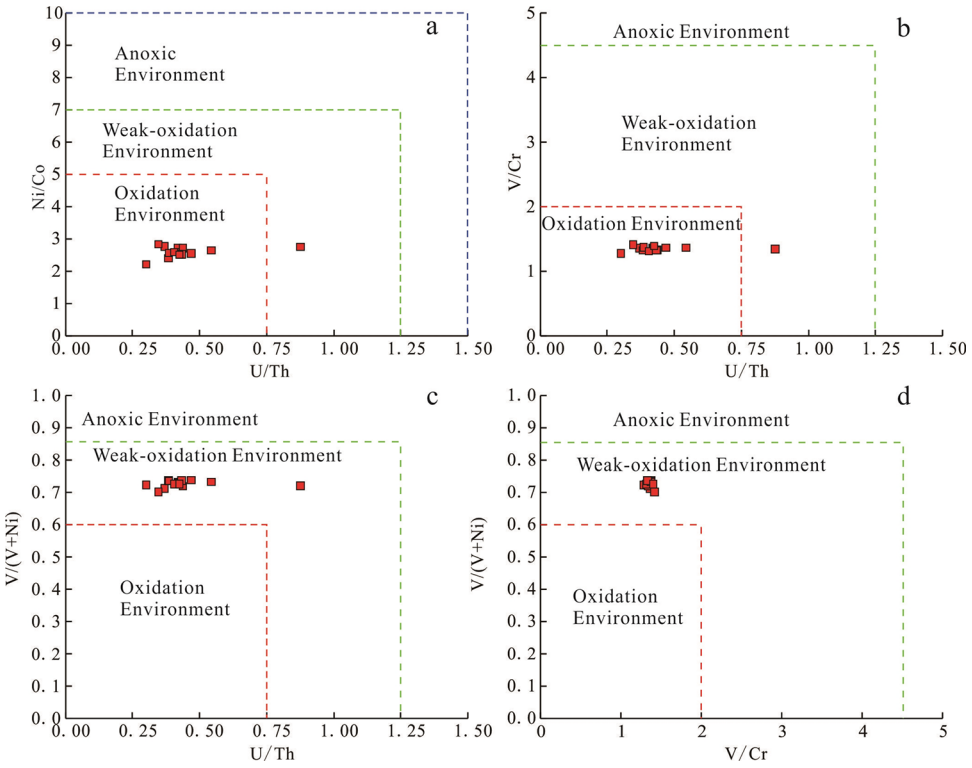

Figure 9. Discrimination index diagram of redox conditions for mud-clast conglomerates in salt rocks of MYJ Fm. from Well L-2, Simao Basin. (a) Ni/Co-U/Th; (b) V/Cr-U/Th; (c) V/(V + Ni)-U/Th; (d) V/(V + Ni)-V/Cr.

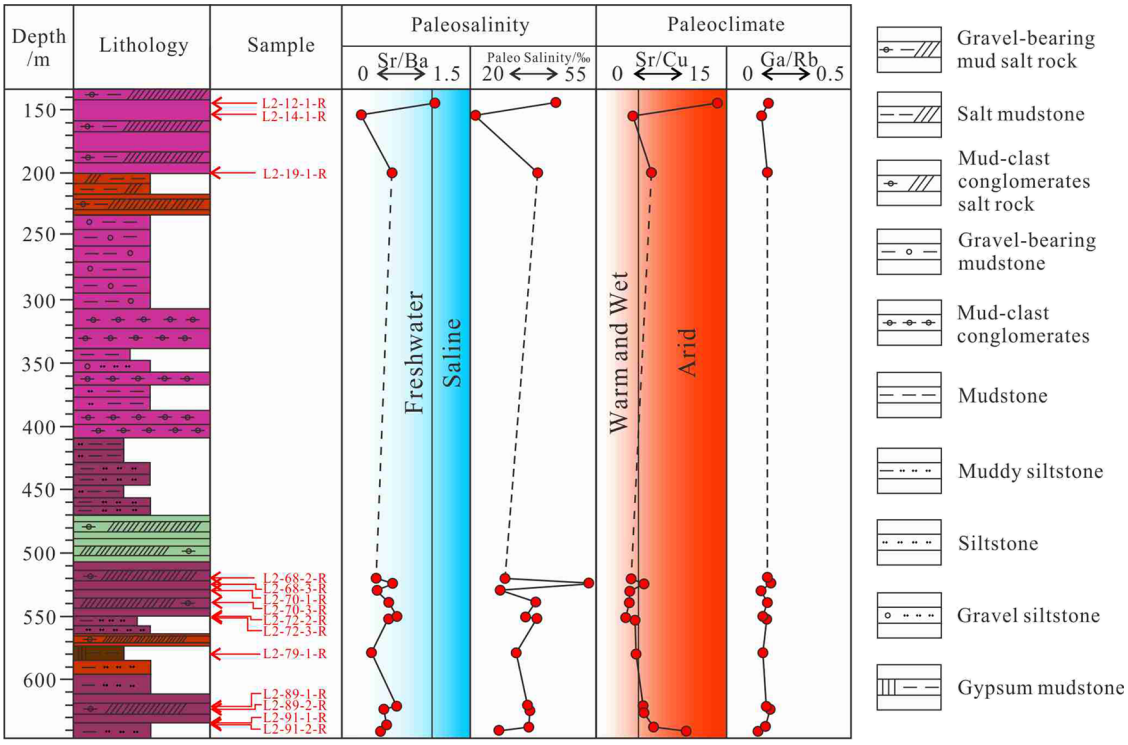

Figure 10. Paleosalinity distribution of mud-clast conglomerates in the salt rocks of MYJ Fm. in the well L-2 is vertical.

$$\log B_k = C_1 \log S_p + C_2 \quad (1)$$

$$B_k = B/(4X_i + 2X_m + X_k) \quad (2)$$

B_K is the boron content of kaolinite (ppm), B is the measured boron content (ppm), X_i, X_m, and X_k are the relative contents of illite, montmorillonite, and kaolinite in clay minerals, S_p is the paleosalinity (‰), and C_1 and C_2 are constant. According to the relationship between the boron content of kaolinite and salinity in modern sedimentary water, C_1 and C_2 are 1.28 and 0.11, respectively.[76]

https://doi.org/10.1021/acsomega.2c00292
ACS Omega 2022, 7, 15547−15560

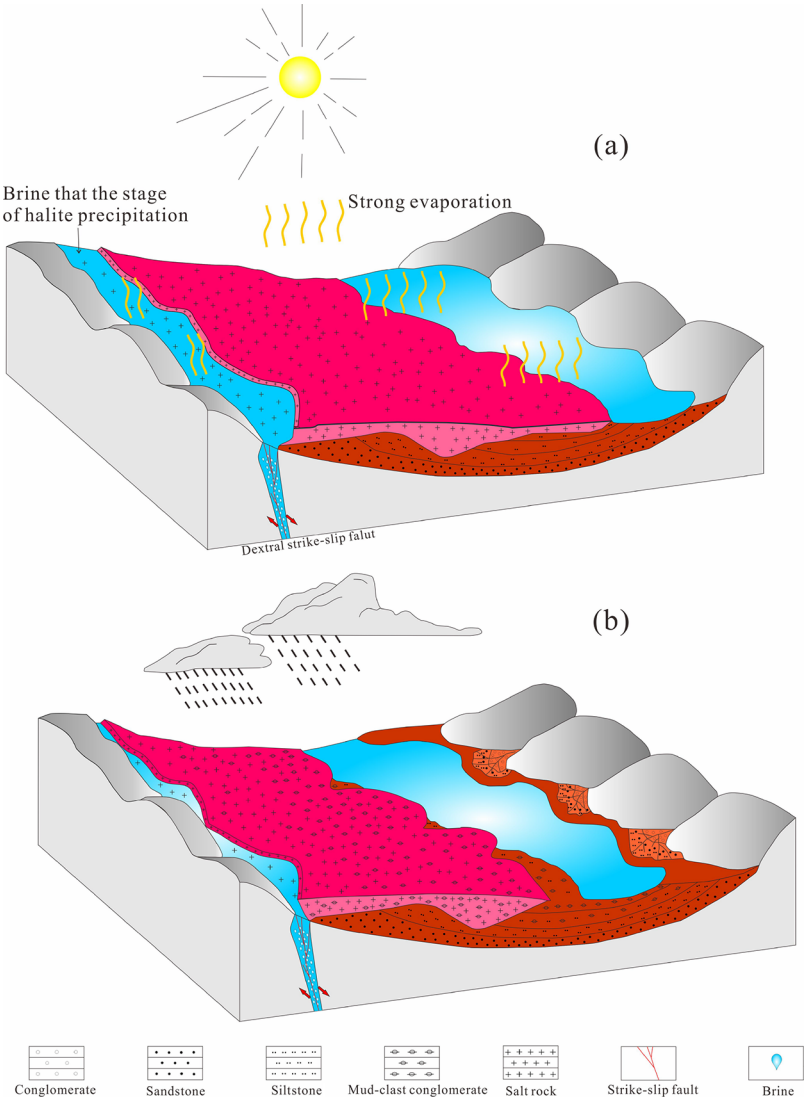

Figure 11. Genetic model of mud-clast conglomerates in salt rocks of MYJ Fm. from well L-2, Simao Basin (Adapted with permission from ref 7, Geology in China 2021) (a) Evaporative and salt precipitation stage. (b) Freshwater replenishment stage.

According to formulas 1 and 2, the paleosalinity distribution of mud-clast conglomerate depositional water in MYJ Fm. of well L-2 ranges from 21‰ to 52‰, with an average value of ∼35‰. The results of quantitative calculation of paleosalinity and Sr/Ba ratio have the same change trend (Figure 10). This result is also verified by the mud-clast conglomerates of MYJ Fm. in the MZK-3 well near the Mengyejing potash mine. According to the boron content calculation, the paleosalinity of the water body during the deposition period of the mud-clast conglomerate ranges from 10‰ to 92‰, with an average of ∼35‰.[21] The paleosalinity value of the mud-clast conglomerates in the MYJ Fm. of the MZK-3 well is close to that of the samples in this paper, which indicates that the salinity of the water bodies did not reach the stage of salt precipitation during the deposition of the clastic rocks in the MYJ Fm.

5.6. Genesis of Mud-Clast Conglomerates in Salt Rocks and Their Salt Mineralization Significance. Based on the existing research results of the basic geology and salt deposit geology of the Simao Basin combined with the results of trace elements and paleosalinity characteristics, the genetic model of the mud-clast conglomerates in the salt rocks of well L-2 may be (Figure 11) in the late Early Cretaceous, and the Simao Basin has evolved into a large continental basin, controlled by deep and large faults, with the good closed condition. At this time, the paleoclimate is generally dry, the evaporation is strengthened, and the brine that has been concentrated to the stage of salt precipitation forms salt rocks under this background. The terrestrial freshwater replenishes the evaporation basin. On the one hand, it desalinates the brine, and on the other hand, the argillaceous debris carried can be used as a protective layer for the early precipitation of salt rock to prevent it from being dissolved. Under the arid climate background, the evaporation rate is much higher than the freshwater supply rate, resulting in the shallower water bodies, and the supply of freshwater also enhances the hydrodynamics in the basin, so that the incompletely consolidated clastic sediments are broken into mud gravel shapes and co-deposited together with the evaporated salts to form mud-clast conglomerate-bearing salt rock. In this way, the process of salt precipitation and desalination alternates, forming a thick layer of mud-clast conglomerate-bearing salt rock. The evidence under the microscope of the desalination−precipitation process is that some of the halite minerals are precipitated in the clastic in the form of crystals.[13]

https://doi.org/10.1021/acsomega.2c00292
ACS Omega 2022, 7, 15547−15560

The interpretation of the genesis of mud-clast conglomerates in salt rocks is of great significance for understanding the genesis of salt deposits: The sedimentary background of salt precipitation is a continental basin, that is, the age of sedimentary salt precipitation is the Late Early Cretaceous, and mud-clast conglomerates deposited with salt have obvious characteristics of terrigenous replenishment, mainly from the Upper Crust felsic material. Before converging to the evaporation basin, the brine has been concentrated to the stage of rock salt precipitation. In the deep middle Jurassic Hepingxiang Fm. of the basin, there is an obvious marine sedimentary background, shell limestone and gypsum rock are developed, and there is a strong indication of salt content. Salt frost and salt springs are all over the region, and most of the solid salt deposits have faults connecting the deep brine bearing strata; therefore, it has the conditions to provide the original brine. In the process of evaporation and salt precipitation, terrestrial freshwater continues to carry debris into the sedimentary basin. This repeated salt precipitation−desalination process causes the salt material deposited in the earlier stage to undergo a process of dissolution−recrystallization, salt with mud-clast conglomerate co-deposition, and mineralization.

6. CONCLUSIONS

(1) The geochemical characteristics of mud-clast conglomerates in the salt rocks of MYJ Fm. indicate that the source of mud-clast conglomerates is terrigenous, belongs to felsic rocks, and derived from the Upper Crust, and the source structure is mainly based on the active continental margin. It has the characteristics of the provenance area supplied by the continental arc. The paleoclimate during the mud-clast conglomerate depositional in the salt rocks of MYJ Fm. is dry and hot as a whole, the warm and humid climate is interspersed in individual periods, and the main sedimentary background is the oxidation environment. The salinity of water bodies in the mud-clast conglomerates depositional period of salt rock is similar to that of current seawater, with an average value of ∼35‰, which is far from reaching the stage of rock salt precipitation.

(2) According to the trace element results of mud-clast conglomerates and the characteristics of paleosalinity, the genetic model may be as follows: The brine that has been concentrated to the stage of precipitating salt evaporates to form salt in a shallow continental basin, and then the terrigenous freshwater input into the basin dissolved the salt rocks, and the debris carried by it formed a protective layer so that the previously deposited salt rocks could not be completely dissolved. In the evaporation basin, brine and freshwater are alternately recharged, and the clastic sediments in the early diagenetic stage broken into mud-clast conglomerates with salt are deposited and mineralized at the same time.

AUTHOR INFORMATION

Corresponding Author

Zhongying Miao − *MNR Key Laboratory of Saline Lake Resources and Environments, Institute of Mineral Resources, Chinese Academy of Geological Sciences, Beijing 100037, China*; Email: zhymiao@foxmail.com

Authors

Pengcheng Lou − *School of Earth Sciences and Resources, China University of Geosciences, Beijing 100083, China*; orcid.org/0000-0002-9246-0885

Mianping Zheng − *MNR Key Laboratory of Saline Lake Resources and Environments, Institute of Mineral Resources, Chinese Academy of Geological Sciences, Beijing 100037, China*

Nina Ma − *MNR Key Laboratory of Saline Lake Resources and Environments, Institute of Mineral Resources, Chinese Academy of Geological Sciences, Beijing 100037, China*

Qihui Xu − *School of Earth Sciences and Resources, China University of Geosciences, Beijing 100083, China*

Xinmin Li − *Institute of Yunnan Geology Survey, Kunming 650051, China*

Complete contact information is available at: https://pubs.acs.org/10.1021/acsomega.2c00292

Notes

The authors declare no competing financial interest.

ACKNOWLEDGMENTS

This work was financially supported by the China Geological Survey Project (DD20201115 and DD20221913).

REFERENCES

(1) Zheng, M.; Zhang, Z.; Yin, H.; Tan, X.; Yu, C.; Shi, L.; Zhang, X.; Yang, J.; Jiao, J.; Wu, G. A New Viewpoint concerning the Formation of the Mengyejing Potash Deposit in Jiangcheng, Yunnan. *Acta Geosci. Sin.* **2014**, *35*, 11−24.

(2) Liu, C.; Wang, L.; Yan, M.; Zhao, Y.; Cao, Y.; Fang, X.; Shen, L.; Wu, C.; Lv, F.; Ding, T. The Mesozoic−Cenozoic tectonic settings, paleogeography and evaporitic sedimentation of Tethyan blocks within China: Implications for potash formation. *Ore Geol. Rev.* **2018**, *102*, 406−425.

(3) Qu, Y.; Yuan, P.; Shuai, K.; Zhang, Y.; Cai, K.; Jia, S.; Chen, C. *Potashforming rules and prospect of the Lower Tertiary in the Lanping-Simao Basin, Yunnan*, 1nd ed.; Jiang, X., Ed.; Geological Press: Beijing, 1998; pp. 1−118.

(4) Li, M.; Yan, M.; Wang, Z.; Liu, X.; Fang, X.; Li, J. The origins of the Mengye potash deposit in the Lanping−Simao Basin, Yunnan Province, Western China. *Ore Geol. Rev.* **2015**, *69*, 174−186.

(5) Miao, Z. New Sr Isotope Evidence to Support the Material Source of the Mengyejing Potash Deposit in the Simao Basin from Ancient Marine Halite or Residual Sea. *Acta Geol. Sin. (Engl. Ed.)* **2018**, *92*, 866−867.

(6) Miao, Z.; Zheng, M.; Zhang, X.; Zhang, Z.; Liu, J.; Gao, Y.; Zhai, X. Sulfur Isotope Geochemistry of the Lower Cretaceous Evaporite and Its Significance for Potash Mineralization in the Simao Basin, Southwest China. *Acta Geosci. Sin.* **2019**, *40*, 279−290.

(7) Miao, Z.; Zheng, M.; Lou, P.; Zhang, X.; Sun, H.; Zhang, Z.; Xu, Q.; Du, X. *A new genetic model for potash deposits of the Simao Basin, Yunnan: Evidence from Sr isotope*; Geology in China 2021, https://kns.cnki.net/kcms/detail/11.1167.P.20201207.1635.006.html.

(8) An, Z.; Xu, J.; Han, J.; He, T. Salt Structural Features and Genetic Mechanism of the Mengyejing Sylvite Deposit in Lanping-Simao Basin, Yunnan. *J. Salt Lake Res.* **2015**, *23*, 15−23.

(9) Wang, L.; Liu, C.; Fei, M.; Shen, L.; Zhang, H.; Zhao, Y. First SHRIMP U−Pb zircon ages of the potash-bearing Mengyejing Formation, Simao Basin, southwestern Yunnan, China. *Cretaceous Res.* **2015**, *52*, 238−250.

(10) Wang, L.; Liu, C.; Shen, L.; Bo, Y. Research Advances in Potash Forming of the Simao Basin, Eastern Tethyan Realm. *Acta Geol. Sin.* **2018**, *92*, 1707−1723.

(11) Yan, M.; Zhang, D.; Fang, X.; Zhang, W.; Song, C.; Liu, C.; Zan, J.; Shen, M. New insights on the age of the Mengyejing Formation in

https://doi.org/10.1021/acsomega.2c00292
ACS Omega 2022, 7, 15547−15560

the Simao Basin, SE Tethyan domain and its geological implications. *Sci. China-Earth Sci.* **2021**, *64*, 231−252.
(12) Shen, L.; Liu, C.; Wang, L.; Hu, Y.; Hu, M.; Feng, Y. Degree of Brine Evaporation and Origin of the Mengyejing Potash Deposit: Evidence from Fluid Inclusions in Halite. *Acta Geol. Sin.-(Engl. Ed.)* **2017**, *91*, 175−185.
(13) Shao, C.; Hu, H.; Yin, H.; Miao, Z.; Zhang, X.; Li, W.; Xia, Z. Characteistics of in situ elemental composition of rock salt from the Simao Basin: New metallogenic insights. *Earth Sci. Front.* **2021**, *28*, 66−78.
(14) Ma, H.; Li, Y.; Cheng, H.; Qing, X.; Zhang, X.; Miao, W.; Xu, J.; Li, B.; Hai, Q. Metallogenic Model and Processes of the Cretaceous Potassium-Bearing Evaporites Involving Changdu, Lanping-Simao and Khorat Basin. *J. Salt Lake Res.* **2019**, *27*, 1−11.
(15) Zheng, M.; Zhang, Z.; Zhang, Y.; Liu, X.; Yin, H. Potash Exploration Characteristics in China: New Understanding and Research Progress. *Acta Geosci. Sin.* **2012**, *33*, 280−294.
(16) Liu, Y.; Zheng, M.; Zhang, Z.; Yu, C.; Miao, Z.; Zhang, K.; Gao, L. Salt Tectonic and Prospecting Potassium Research in Simao Basin. *Geol. Rev.* **2017**, *63*, 568−580.
(17) Tang, Q.; Zhang, X.; Miao, W.; Ma, H.; Li, Y.; Li, W.; Yuan, X. Mineralogical characteristics and sedimentary envrionment significance of water-insoluble minerals in potash deposits of Vientiane Basin of Laos. *Carbonates Evaporites* **2021**, *36*, 70.
(18) Xu, Y.; Cao, Y.; Liu, C.; Jiao, P. Provenance and Degree of Evaporation and Concentration of Eocene Salt Lake in the Kuqa Basin. *Acta Geol. Sin.* **2018**, *92*, 1617−1629.
(19) Miao, W.; Ma, H.; Zhang, X.; Zhang, Y.; Li, Y. Clay Mineral Characteristics of Salt Sequence in Drill Hole SHK4 of the Mengyejing Potassium Deposit of Jiangcheng, Lanping-Simao Basin, Yunnan Province, and Their Sylvite-forming Significance. *Acta Geosci. Sin.* **2013**, *34*, 537−546.
(20) Miao, W.; Ma, H.; Zhang, X.; Shi, H.; Li, Y.; Rong, Z. Mineralogical and Geochemical Characteristics of Detrital Rocks in the Mengyejing Formation and Evolution of the Sedimentary Environment of Paleolake in Simao Basin, Yunnan Province. *Acta Geol. Sin.* **2015**, *89*, 2096−2107.
(21) Lou, P.; Miao, Z.; Zheng, M.; Zhang, X.; Ruan, Z.; Xu, Q. Paleogeographic Characteristics of the Mengyejing Formation in the Simao Basin during Its Depositional Period and Its Indication of Potash Mineralization: A Case Study of MZK-3 Well. *Minerals* **2021**, *11*, 338.
(22) Shi, H. Y.; Ma, H. Z.; Miao, W. L.; Li, Y.; Zhang, X. Characteristics and geological significances of rare earth and trace elements from Upper Cretaceous Mengyejing Formation of Simao Basin in Jiangcheng County, Yunnan Province. *Geochimica* **2014**, *43*, 415−427.
(23) Metcalfe, I. Permian tectonic framework and palaeogeography of SE Asia. *J. Asian Earth Sci.* **2002**, *20*, 551−566.
(24) Sone, M.; Metcalfe, I. Parallel Tethyan sutures in mainland Southeast Asia: New insights for Palaeo-Tethys closure and implications for the Indosinian orogeny. *C. R. Geosci.* **2008**, *340*, 166−179.
(25) Liao, Z.; Chen, Y. Nature and Evolution of Lanping-Simao Basin Prototype. *J. Tongji Univ.* **2005**, *33*, 1527−1531.
(26) Haihong, C.; Dobson, J.; Heller, F.; Jie, H. Paleomagnetic evidence for clockwise rotation of the Simao region since the Cretaceous: A consequence of India-Asia collision. *Earth Planet. Sci. Lett.* **1995**, *134*, 203−217.
(27) Sato, K.; Liu, Y.; Zhu, Z.; Yang, Z.; Otofuji, Y. Paleomagnetic study of middle Cretaceous rocks from Yunlong, western Yunnan, China: evidence of southward displacement of Indochina. *Earth Planet. Sci. Lett.* **1999**, *165*, 1−15.
(28) Sato, K.; Liu, Y.; Wang, Y.; Yokoyama, M.; Yoshioka, S.; Yang, Z.; Otofuji, Y.-I. Paleomagnetic study of Cretaceous rocks from Pu'er, western Yunnan, China: Evidence of internal deformation of the Indochina block. *Earth Planet. Sci. Lett.* **2007**, *258*, 1−15.
(29) Tong, Y.-B.; Yang, Z.; Zheng, L.-D.; Xu, Y.-L.; Wang, H.; Gao, L.; Hu, X.-Z. Internal crustal deformation in the northern part of Shan-Thai Block: New evidence from paleomagnetic results of Cretaceous and Paleogene redbeds. *Tectonophysics* **2013**, *608*, 1138−1158.
(30) Yin, H.; Wu, S.; Du, Y.; Peng, Y. South China defined as part of tethyan archipelagic ocean system. *Earth Sci. - J. China Univ. Geosci.* **1999**, *24*, 1−10.
(31) Chen, Y.; Liao, Z.; Wei, Z.; Li, M. Characteristics and tectonic evolution of the Lanping-Simao Mesozoic Basin. *Pet. Geol. Exp.* **2004**, *26*, 219−222.
(32) Yuan, Q.; Qin, Z.; Wei, H.; Sheng, S.; Shan, F. The Ore-forming Age and Palaeoenvironment of the Mengyejing Formation in Jiangcheng, Yunnan Province. *Acta Geosci. Sin.* **2013**, *34*, 631−637.
(33) Li, Y.; Wang, Z.; Wu, P.; Meng, S. Paleoenvironment reconstruction of the upper Paleozoic in the Linxing area, northeastern Ordos Basin, China. *AAPG Bull.* **2021**, *105*, 2545−2574.
(34) Li, Y.; Wang, Z.; Gan, Q.; Niu, X.; Xu, W. Paleoenvironmental conditions and organic matter accumulation in Upper Paleozoic organic-rich rocks in the east margin of the Ordos Basin, China. *Fuel* **2019**, *252*, 172−187.
(35) Tribovillard, N.; Algeo, T. J.; Lyons, T.; Riboulleau, A. Trace metals as paleoredox and paleoproductivity proxies: An update. *Chem. Geol.* **2006**, *232*, 12−32.
(36) Brumsack, H. J. The inorganic geochemistry of Cretaceous black shales (DSDP Leg 41) in comparison to modern upwelling sediments from the Gulf of California. *Geological Society, London, Special Publications* **1986**, *21*, 447−462.
(37) Calvert, S. E.; Pedersen, T. F. Geochemistry of recent oxic and anoxic marine-sediments - implications for the geological record. *Mar. Geol.* **1993**, *113*, 67−88.
(38) Morford, J. L.; Emerson, S. The geochemistry of redox sensitive trace metals in sediments. *Geochim. Cosmochim. Acta* **1999**, *63*, 1735−1750.
(39) Piper, D. Z.; Perkins, R. B. A modern vs. Permian black shale—the hydrography, primary productivity, and water-column chemistry of deposition. *Chem. Geol.* **2004**, *206*, 177−197.
(40) Liyuan, W.; Qingjun, G.; Changqiu, Z.; Rongfei, W.; Yinan, D.; Xiaokun, H.; Liyan, T.; Jing, K.; Xi, Y. Trace and rare earth elements geochemistry of sedimentary rocks in the Ediacaran-Cambrian transition from the Tarim Basin, Northwest China: Constraints for redox environments. *Precambrian Res.* **2021**, *352*, 105942.
(41) Turekian, K. K.; Wedepohl, K. H. Distribution of the Elements in Some Major Units of the Earth's Crust. *Geol. Soc. Am. Bull.* **1961**, *72*, 175−191.
(42) Taylor, S. R.; Mclennan, S. M. The continental crust: its composition and evolution. *J. Geol.* **1985**, *94*, 57−72.
(43) Boynton, W. V. Cosmochemistry of the Rare Earth Elements: Meteorite Studies. *Dev. Geochem.* **1984**, *2*, 63−114.
(44) Haskin, M. A.; Haskin, L. A. Rare Earths in European Shales: A Redetermination. *Science* **1966**, *154*, 507−509.
(45) Lerman, A. *Lakes: Chemistry, Geology, Physics*; 1nd ed.; Tu, Y. Ed.; Geological Press: Beijing, 1989; pp. 10−100.
(46) Lee, J. H.; Byrne, R. H. Examination of comparative rare earth element complexation behavior using linear free-energy relationships. *Geochim. Cosmochim. Acta* **1992**, *56*, 1127−1137.
(47) Kong, W. L.; Wang, S.; Du, Y.-L.; Wan, Q.; Li, S.-Y. Composition and geochemistry of Permian clastic rocks in the northern margin of the Middle and Upper Yangtze region. *Geochimica* **2011**, *40*, 473−486.
(48) Li, S.; Wang, Q. Geochemical characteristics of Tertiary mudstones in Kuqa depression and their implications to tectonic setting and provenance attribute. *Acta Petrol. Mineral.* **2006**, *25*, 219−229.
(49) Li, Z.; Liu, J.; Hu, R.; Liu, Y.; Li, C.; He, M. Tectonic Setting and Provenance of Source Rock for Sedimentary Rocks in Lanping Mesozoic-Cenozoic Basin: evidences from geochemistry of sandstones. *Acta Sedimentol. Sin.* **2003**, *21*, 547−552.
(50) Shields, G.; Stille, P. Diagenetic constraints on the use of cerium anomalies as palaeoseawater redox proxies: an isotopic and REE study of Cambrian phosphorites. *Chem. Geol.* **2001**, *175*, 29−48.

https://doi.org/10.1021/acsomega.2c00292
ACS Omega 2022, 7, 15547−15560

(51) Mclennan, S. M. Rare earth elements in sedimentary rocks: influence of provenance and sedimentary processes. *Rev Mineral. Geochem.* **1989**, *21*, 169−200.
(52) Floyd, P. A.; Leveridge, B. E. Tectonic environment of the Devonian Gramscatho basin, south Cornwall: framework mode and geochemical evidence from turbiditic sandstones. *J. Geol. Soc.* **1987**, *144*, 531−542.
(53) Gu, X. X.; Liu, J. M.; Zheng, M. H.; Tang, J. X.; Qi, L. Provenance and Tectonic Setting of the Proterozoic Turbidites in Hunan, South China: Geochemical Evidence. *J. Sediment. Res.* **2002**, *72*, 393−407.
(54) Allègre, C. J.; Minster, J. F. Quantitative models of trace element behavior in magmatic processes. *Earth Planet. Sci. Lett.* **1978**, *38*, 1−25.
(55) Veizer, J.; Mackenzie, F. T. Evolution of sedimentary rocks. *Treatise Geochem. (2nd Ed.)* **2014**, *9*, 399−435.
(56) Bhatia, M. R.; Crook, K. A. W. Trace element characteristics of graywackes and tectonic setting discrimination of sedimentary basins. *Contrib. Mineral. Petrol.* **1986**, *92*, 181−193.
(57) Xu, D.; Ma, C.; Nonna, B. C.; Li, P.; Xia, B.; Zhang, Y. Petrological, mineralogical and geochemical characteristics of Ordovician volcanic-clastic sedimentary rocks in Bangxi area, Northwest Hainan Island, South China: Implications for provenance and tectonic setting. *Geochimica* **2007**, *36*, 11−26.
(58) Roy, D. K.; Roser, B. P. Climatic control on the composition of Carboniferous−Permian Gondwana sediments, Khalaspir basin, Bangladesh. *Gondwana Res.* **2013**, *23*, 1163−1171.
(59) Beckmann, B.; Flogel, S.; Hofmann, P.; Schulz, M.; Wagner, T. Orbital forcing of Cretaceous river discharge in tropical Africa and ocean response. *Nature* **2005**, *437*, 241−244.
(60) Cao, H.; Guo, W.; Shan, X.; Ma, L.; Sun, P. Paleolimnological environments and organic accumulation of the nenjiang formation in the southeastern Songliao Basin, China. *Oil Shale* **2015**, *32*, 5−24.
(61) Sarki Yandoka, B. M.; Abdullah, W. H.; Abubakar, M. B.; Hakimi, M. H.; Adegoke, A. K. Geochemical characterisation of Early Cretaceous lacustrine sediments of Bima Formation, Yola Sub-basin, Northern Benue Trough, NE Nigeria: Organic matter input, preservation, paleoenvironment and palaeoclimatic conditions. *Mar. Pet. Geol.* **2015**, *61*, 82−94.
(62) Singer, A. The Paleoclimatic interpretation of clay minerals in sediments—A review. *Earth-Sci. Rev.* **1984**, *21*, 251−293.
(63) Gingele, F. X.; De Deckker, P.; Hillenbrand, C. D. Late Quaternary fluctuations of the Leeuwin Current and palaeoclimates on the adjacent land masses: clay mineral evidence. *Aust. J. Earth Sci.* **2001**, *48*, 867−874.
(64) Vanderaveroet, P. Miocene to Pleistocene clay mineral sedimentation on the New Jersey shelf. *Oceanol. Acta* **2000**, *23*, 25−36.
(65) Huang, K.; Opdyke, N. D. Paleomagnetic results from Cretaceous and Jurassic rocks of South and Southwest Yunnan: evidence for large clockwise rotations in the Indochina and Shan-Thai-Malay terranes. *Earth Planet. Sci. Lett.* **1993**, *117*, 507−524.
(66) Wu, C.; Liu, C.; Yi, H.; Xia, G.; Zhang, H.; Wang, L.; Li, G.; Wagreich, M. Mid-Cretaceous desert system in the Simao Basin, southwestern China, and its implications for sea-level change during a greenhouse climate. *Paleogeogr. Paleoclimatol. Paleoecol.* **2017**, *468*, 529−544.
(67) Zhao, Y.; Liu, C.; Zhang, H.; Li, Z.; Ding, T.; Wang, M. The controls of paleotemperature on potassium salt precipitation in ancient salt lakes. *Acta Petrol. Sin.* **2015**, *31*, 2751−2756.
(68) Boucot, A. J.; Xu, C.; Scotese, C. R.; Morley, R. J. *Phanerozoic Paleoclimate: An Atlas of Lithologic Indicators of Climate, Digital Version*; Nichols, G. J., Ed.; SEPM Society for Sedimentary Geology: Oklahoma, 2013; pp. 214−231.
(69) Kimura, H.; Watanabe, Y. Ocean anoxia at the Precambrian−Cambrian boundary. *Geology* **2001**, *29*, 995−998.
(70) Jones, B.; Manning, D. A. C. Comparison of geochemical indexes used for the interpretation of palaeoredox conditions in ancient mudstones. *Chem. Geol.* **1994**, *111*, 111−129.
(71) Dill, H. Metallogenesis of early Paleozoic graptolite shales from the Graefenthal horst (Northern Bavaria-Federal-Republic-of-Germany). *Econ. Geol.* **1986**, *81*, 889−903.
(72) Algeo, T. J.; Maynard, J. B. Trace-element behavior and redox facies in core shales of Upper Pennsylvanian Kansas-type cyclothems. *Chem. Geol.* **2004**, *206*, 289−318.
(73) Rimmer, S. M.; Thompson, J. A.; Goodnight, S. A.; Robl, T. L. Multiple controls on the preservation of organic matter in Devonian−Mississippian marine black shales: geochemical and petrographic evidence. *Paleogeogr. Paleoclimatol. Paleoecol.* **2004**, *215*, 125−154.
(74) Pattan, J. N.; Pearce, N. J. G.; Mislankar, P. G. Constraints in using Cerium-anomaly of bulk sediments as an indicator of paleo bottom water redox environment: A case study from the Central Indian Ocean Basin. *Chem. Geol.* **2005**, *221*, 260−278.
(75) Hatch, J. R.; Leventhal, J. S. Relationship between inferred redox potential of the depositional environment and geochemistry of the Upper Pennsylvanian (Missourian) Stark Shale Member of the Dennis Limestone, Wabaunsee County, Kansas. *U.S.A. Chem. Geol.* **1992**, *99*, 65−82.
(76) Couch, E. L. Calculation of Paleosalinities from Boron and Clay Mineral Data. *AAPG Bull.* **1971**, *55*, 1829−1837.

https://doi.org/10.1021/acsomega.2c00292
ACS Omega 2022, 7, 15547−15560